Real-Time Generation of Arias Intensity and Seismic Landslides Hazards Maps Using GIS

M. Mahdavifar[1], M.K. Jafari[2], and M.R. Zolfaghari[3]

1. Assistant Professor, Geotechnical Engineering Research Center, International Institute of Earthquake Engineering and Seismology, I.R. Iran, email: mahdavif@iiees.ac.ir
2. Professor, Geotechnical Engineering Research Center, International Institute of Earthquake Engineering and Seismology, Tehran, I.R. Iran
3. Assistant Professor, Civil Engineering Department, Khajeh Nasir Toosi University of Technology, Tehran, I.R. Iran

ABSTRACT: *A GIS-based platform is developed by which shaking intensity and seismic landslide hazard zonation maps are generated in a short time after the earthquake. The shaking over the entire regional extent of earthquake prone area is obtained by Arias intensity attenuation relationship. By using simplified Newmark method, the seismic landslide hazard zonation map is generated based on the calculated Newmark's displacements.*

Keywords: Landslide; Landslides triggered by earthquake; Arias Intensity map; Landslide hazard zonation

1. Introduction

The most common information available immediately following a damaging earthquake is its magnitude and epicentral location. However, the damage pattern is not a simple function of these two parameters alone, and more detailed information must be provided to properly ascertain the situation [24]. We currently generate a primary version of a *GIS*-base system which can provide the map of Arias intensity (based on proposed attenuation relationships, e.g. [18]), as well as a map for seismic landslide hazard zonation, based on simplified Newmark's displacement method [17] in a short time after an earthquake. These maps provide a rapid portrayal of the extent of potentially damaging shaking following an earthquake and can be used for emergency response efforts, loss estimation models, and for public information through the media. Generation of such maps is fully automatic, triggered by any significant earthquake. The platform is calibrated using data from the 1990 Manjil earthquake, $Mw = 7.1$, and it's application is demonstrated in the area covered by Cholkasar and Chaharmahal quadrangles, on the southeast of the earthquake epicenter.

2. Study Area

From strong ground motion points of view, the Iranian territory can be divided into two tectonic provinces, see Figure (1). The Zagros thrust fault zone is the main geological frontier, separating the Arabian plate from the central Iran micro plate, between the Zagros and non-Zagros regions. The seismic history in Zagros reveals more frequent earthquakes but with relatively lower severity than other areas including Central Iran plate. In this region seismic energy is released mostly by earthquakes in the middle range magnitude (M4-6). In the Alborz and Central Iran zones, the earthquakes are less frequent but with relatively higher magnitude than those in Zagros. Such destructive earthquakes have shaken the country in the recent decades, examples are the Tabas earthquake (1978, Central-Iran) and the Manjil earthquake (1990, Alborz) [27].

3. Newmark's Displacement Method

A principal cause of earthquake damage is landsliding, and the ability to predict earthquake-triggering landslide displacements is important for many types of seismic-hazard analyses and for the design of engineered slopes. Newmark's method for modeling a landslide as a rigid-plastic block sliding on an inclined plane provides a workable means of predicting

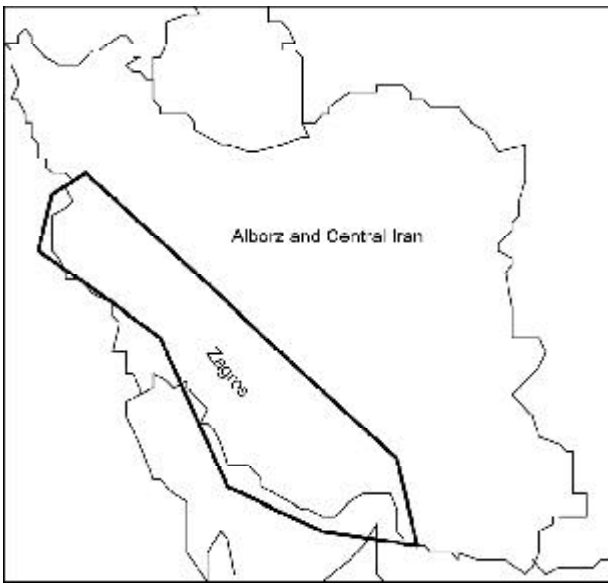

Figure 1. Iran could be divided into two regions: Zagros region (the area, which is limited by heavy, solid line) and Alborz and Central Iran region (the rest area of Iran) [22].

approximate landslide displacements. The sliding block analogy inherently assumes (1) rigid perfectly-plastic behavior (2) the existence of well defined slip surface, (3) negligible loss in shear resistance during shaking and (4) permanent displacement occurs only if dynamic stresses exceed shear resistance [21].

Applying Newmark's method requires knowing the yield or critical acceleration of the landslide (above which permanent displacement occurs), which can be determined from the static factor of safety and from the landslide geometry [12]. Assuming negligible loss in shear resistance during shaking, the critical acceleration in terms of gravity, a_c, for a slope with planar slip can be determined with

$$a_c = (FS - 1)\sin\alpha \quad (1)$$

where FS is the static factor of safety, and α (thrust angle) is the angle between the slip direction of the center of mass and the horizontal [19].

For the simplest model of an infinite slope (planner slip surface parallel to the slope), the static factor of safety can be expressed as:

$$FS = \frac{c'}{\gamma t \sin\alpha} + \left(1 - m\frac{\gamma_W}{\gamma}\right)\frac{\tan\phi'}{\tan\alpha} \quad (2)$$

where c' is the effective cohesion, ϕ' is the effective angle of internal friction, γ is the material unit weight, t is the slope-normal thickness of the failure slab, and m is the proportion of t that is saturated [11, 14].

The assumption of infinite slope failure is valid if 1) the landslide mass is thin compared to its length; 2) the failure surface is parallel to the ground surface; 3) failure occurs as basal sliding [11].

The conventional Newmark analysis calculates the cumulative displacement, D_N, of the friction block as it is subjected to the acceleration of a given earthquake time history. This is done by double-integrating over those parts of the horizontal earthquake time-history that exceed the critical acceleration [25], see Figure (2).

To avoid the computation complexity and difficulties of selecting an appropriate earthquake time-history, many researchers [e.g. 2, 12, 13, 14, 20] have proposed models that predict Newmark's displacement as a function of ground motion parameters (such as peak ground acceleration, Arias intensity) and site/slope parameters. Jibson [12] developed simplified Newmark model which calculates mean Newmark's displacement, D_N, using a simple regression model:

$$Log\, D_N = A\, log\, I_a + B\, a_c + C + /- \sigma \quad (3)$$

where D_N is Newmark displacement, I_a is Arias intensity, a_c is critical acceleration, and A, B, C are

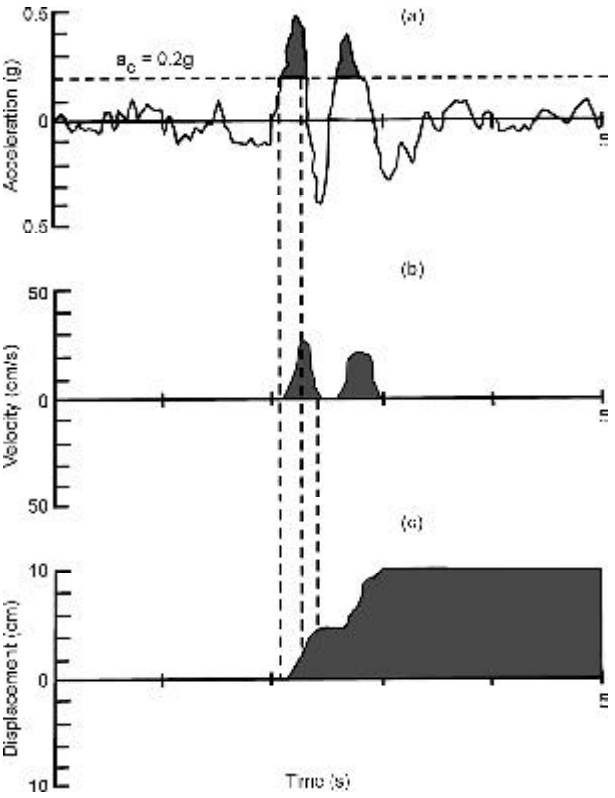

Figure 2. Demonstration of the Newmark-analysis algorithm (adapted from Wilson and Keefer [25]). A: Earthquake acceleration-time history with critical acceleration (horizontal dashed line) of 0.20g superimposed. B: Velocity of landslide block versus time. C: Displacement of landslide block versus time [14].

regression coefficients and σ is estimated standard deviation of the model. The functional form of the model was modified by Jibson et al [14] and Jibson [13] as below to make the critical acceleration term logarithmic:

$$Log\, D_N = A \log I_a + B \log a_c + C +/- \sigma \quad (4)$$

Mahdavifar [17] using both models regressed data from Alborz and Central Iran and developed two equations below:

$$Log\, D_N = 1.087 \log I_a - 7.176\, a_c + 1.398 ; \sigma Log\, D_N = 0.397 \quad (5)$$

$$Log\, D_N = 1.207 \log I_a - 1.876 \log a_c + 1.608 ; \sigma Log\, D_N = 0.380 \quad (6)$$

The regression models were trained using 105 earthquake records, with Arias Intensity ranging from 0.06-3*m/s.* Newmark's displacement were calculated over a limited range of critical acceleration (0.02-0.4*g*) using each earthquake record. Since using a linear term for a_c makes the equation overly sensitive to small changes in displacement, the Eq. (6) is selected for this study. Also Mahdavifar et al [18] suggested the following attenuation relationship to predict Arias intensity:

$$Log\, I_a = 0.810 M - \log R - 0.002 R - 3.880 ; \sigma Log\, I_a = 0.460 \quad (7)$$

where I_a is Arias intensity in *m/sec*, M is moment magnitude, and R is the closest distance from the site to the surface trace of earthquake fault if the fault is known, otherwise R is the hypocentral distance.

4. Shear-Strength Parameters

Determining the representative shear-strength values for geological units is necessary to calculate the factor of safety of slope, see Eq. (2). Wilson and Keefer [25] have grouped the various types of slope materials into three broad lithologic categories, each having assumed average values of c' and F', see Figure (3).

Geological Strength Index (*GSI*) introduced by Hoek [6], Hoek and Brown [7], and Hoek et al [8-9] provide a system for estimating the reduction in rock mass strength for different geological conditions as identified by field observations. The rock mass characterization is straightforward and it is based upon the visual compression of the rock structure, in terms of blockiness, and the surface condition of the discontinuities indicated by joint roughness and alteration, see Table (1). The combination of these two parameters provides practical basis for describing a wide range of rock mass types, with diversified rock structure ranging from very tightly interlocked strong rock fragments to heavily crushed rock masses. Based on the rock mass description the value

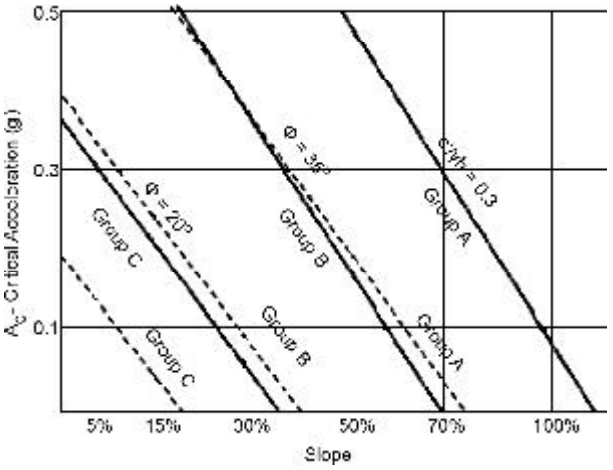

Figure 3. Plots of critical acceleration (Ac) versus slope steepness for three sets of lithologies: group A, strongly cemented rocks (crystalline rock and well-cemented sandstone); group B, weakly cemented rocks (sandy soil and poorly cemented sandstone); group C, argillaceous rocks (clayey soil and shale). The cohesion factor c'/ γ h, for group A assumes values of c= 300psf, γ = 100 pcf, and h=10ft. The angle of internal friction (F) (peak strength, undrained condition) is 35° for sands, sandstone, and crystalline rocks and 20° for clayey soils and shales. The solid lines depict dry slope materials and the dashed lines depict saturation from the slide plane to the surface [25].

Table 1. Characterization of rock masses on the basis of inter locking and joint alteration (based on Hoek and Brown [7]).

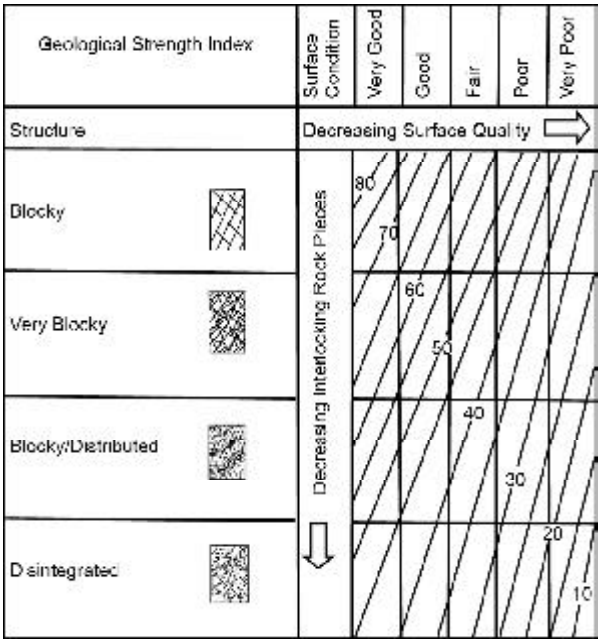

of Geological Strength Index (*GSI*) is estimated from the contours given in Table (1).

The uniaxial compressive strength σ_{ci} and the material constant m_i are determined by laboratory testing or estimated from published tables, see Table (2) and (3). The shear strength of the rock mass, defined by the angle of internal friction φ and cohesion *c*, is estimated from the curves plotted in Figures (4) and (5), [8].

In the methodology proposed in this study, the shear-strength values for rock formations are mainly determined using the Geological Strength Index (*GSI*), and the strength parameters values for non-rock formations are determined using the strength parameters mentioned for similar geological unit (such as [14, 25, 26]).

5. Proposed Analytical Software Tool

Researchers and practitioners in the filed of natural hazards have recognized Geographic Information Systems (*GIS*) to be a significant tool in modeling spatial phonemes related to hazard and risk [19]. In this study a *GIS*-based system is prepared by which real time shaking intensity and seismic landslide hazard zonation maps can be generated in a short time after the earthquake.

Table 2. Field estimates of the uniaxial compressive strength of intact rock pieces [10].

Grade[a]	Term	Uniaxial Compressive Strength (MPa)	Point Load Index (MPa)	Field Estimate of Strength	Examples
R6	Extremely Strong	>250	>10	Specimen can only be chipped with a geological hammer	Fresh Basalt, Chert, Diabase, Gneiss, Granite, Quartzite
R5	Very Strong	100-250	4-10	Specimen requires many blows of geological hammer to fracture it	Amphibolite, Sandstone, Basalt, Gabbro, Gneiss, Granodiorite, Limestone, Marble, Rhyolite, Tuff
R4	Strong	50-100	2-4	Specimen requires more than one blow of a geological hammer to fracture it	Limestone, Marble, Phyllite, Sandstone, Schist, Shale
R3	Medium Strong	25-50	1-2	Can not be scarped or peeled with a pocket knife, specimen can be fractured with a single blow from a geological hammer	Claystone, Coal, Concrete, Schist, Shale, Siltstone
R2	Weak	5-25	[b]	Can be peeled with a pocket knife with difficulty, shallow indentation made by firm blow with point of a geological hammer	Chalk, Rocksalt, Potash
R1	Very Weak	1-5	[b]	Crumbles under firm blows with point of a geological hammer can be peeled by a pocket knife	Highly Weathered or Altered Rock
R0	Extremely Weak	0.25-1	[b]	Indented by thumbnail	Stiff Fault Gouge

[a] Grade according to Brown [3].
[b] Point load tests on rocks with a uniaxial compressive strength below 25 MPa are likely to yield ambiguous results.

Table 3. Values of the constant m_i for intact rock, by rock group. Note that values in parenthesis are estimates [10].

Rock Name	m_i	Rock Name	m_i	Rock Name	m_i	Rock Name	m_i
Conglomerate	(22)	Micritic limestone	8	Gneiss	33	Diorite	(28)
Sandstone	19	Gypstone	16	Schists	4-8	Andesite	19
Siltstone	9	Anhydrite	13	Phyllites	(10)	Gabbro	27
Claystone	4	Marble	9	Slate	9	Dolerite	(19)
Greywacke	(18)	Hornfels	(19)	Granite	33	Basalt	(17)
Chalk	7	Quartzite	24	Rhyolite	(16)	Norite	22
Coal	(8-21)	Migmatite	30	Obsidian	(19)	Agglomerate	(20)
Breccia	20	Amphibolite	25-31	Granodiorite	30	Breccia	(18)
Sparitic Limestone	10	Mylonites	6	Dacite	17	Tuff	(15)

These values are for intact rock specimens tested normal to bedding or foliation. The value of m_i will be significantly different if failure occurs along a weakness plane.

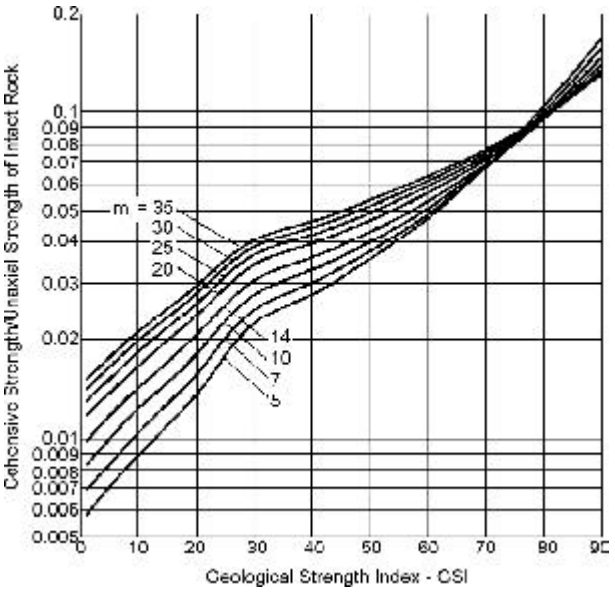

Figure 4. Relationship between cohesive strength and GSI [10].

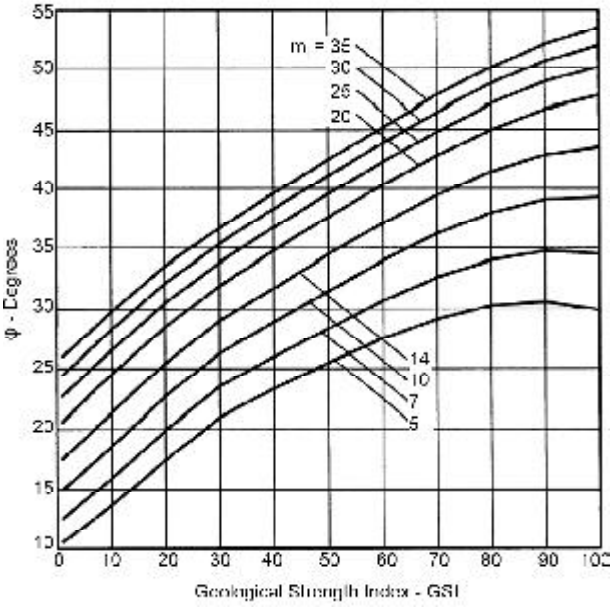

Figure 5. Relationship between friction angle (φ) and GSI [10].

Figure (6) shows the flowchart for the software tool which was developed in this study. As could be seen in this figure, the software tool includes 3 sections: 1) server, 2) database and 3) program and sub programs (surrounded by dashed line). Database includes latitude and longitude of the center of all the morphological units (described in the below), as well as their critical accelerations. For preparation of the database, a Digital Elevation Model (*DEM*) of the Alborz and Central Iran by resolution of 10*m* is needed. The *DEM* is generated using digital topographic maps in the scale of 1:25000. This information is being prepared by National Cartographic Center (*NCC*). For

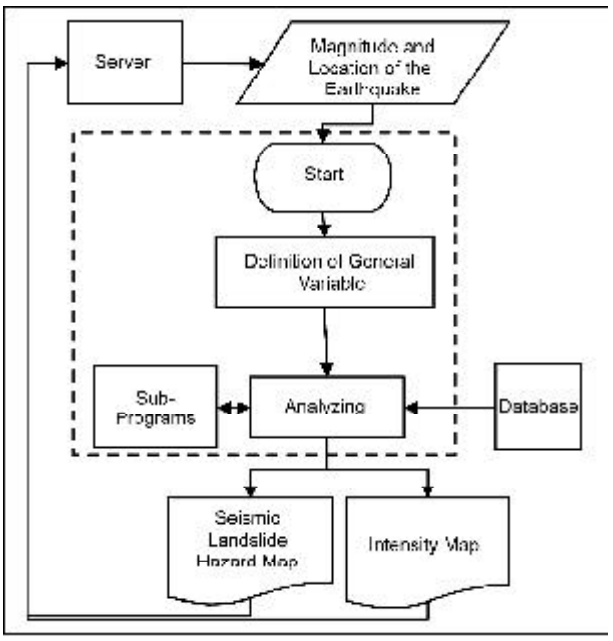

Figure 6. The flowchart of the developed software tool which includes 3 parts: server, database, and program and sub programs (surrounded by dashed line).

this study, we started with some regions which their digital information were available. The *DEM* converted, first, into a triangular irregular network (*TIN*) and then into a polygon coverage having an attribute of slope in degrees from the horizontal and slope direction. The resulted polygons, which have a definite slope and slope direction were used as morphological units.

Data requirement for critical acceleration, a_c, includes soil parameters (c', F', and γ), the slope steepness (α), the ratio indicating the location of the groundwater, m, and slope-normal thickness of the failure slab, t. The coverage of soil parameters are prepared using the procedures presented in section 4. Also for simplicity, m and t are taken to be 0 and 3.5, respectively. These are from the landslides characteristics of Alborz and Central Iran [16]. Finally by overlaying the strength parameters coverage and slope coverage and using Eqs. (1) and (2) the critical acceleration coverage of Alborz and Central Iran and its attribute table is prepared and used as the database.

When a damaging earthquake occurs, the server activates the program and sends earthquake magnitude and epicentral location. The program selects the units of database which are located in earthquake prone area. In the next step, the probable fault of the earthquake is determined, and using Arias intensity attenuation relationship, see Eq. (7), the Arias intensity coverage is generated for the affected area. To determine source to site distance, the nearest horizontal distance between the center of polygons and the fault trace is calculated.

If there is not any active fault near the earthquake epicenter, the epicentral distance is used as source to site distance. By jointing the Arias intensity and critical acceleration coverages and using Eq. (6), the Newmark's displacement converge is created.

After completing the analyses, Arias intensity and Newmark's displacement were arbitrarily categorized into ranges. A graphic module is used to plot maps of intensity and displacement hazard with various thematic views. In Newmark's displacement map (which is named as seismic landslide hazard zonation map), polygons having a slope less than five degree are not analyzed to minimize analysis times and are indicated with light yellow. In the last step, the program sends intensity map and seismic landslide hazard maps, as shape format to server for locating in the web.

6. The Manjil Earthquake Case Study

The study area has not experienced any large earthquake since the developed software tool is developed. Therefore, to test the system, it was performed using the 1990 Manjil earthquake as a real time scenario event. Figure (7) shows intensity map of the 1990 Manjil earthquake (Mw = 7.1). The characteristics of this earthquake are illustrated in Table (4).

Table 4. Characteristics of the Manjil earthquake [23].

Date	Time (GMT)	Longitude	Latitude	Mag. (Ms)	Depth (km)
1990/6/20	21:00:09	49.41	36.96	7.7	18

The Manjil earthquake has induced 120 large landslides and many rock-falls in the epicentral area and vicinity of the earthquake fault [15]. Most documented landslides are those are large enough to locate, and there is not a complete seismic landslide inventory map which show all rock falls and small slides triggered during Manjil earthquake. In this study, Cholkasar and Chaharmahal quadrangles, which cover southeastern part of the Manjill earthquake prone area, are selected for calibration of the system. The Manjil earthquake source data including epicenter and the magnitude have been used as inputs and the system generated intensity map, see Figure (8), and seismic landslide hazard map, see Figure (9), as outputs.

By comparing Figures (7) and (8), it could be

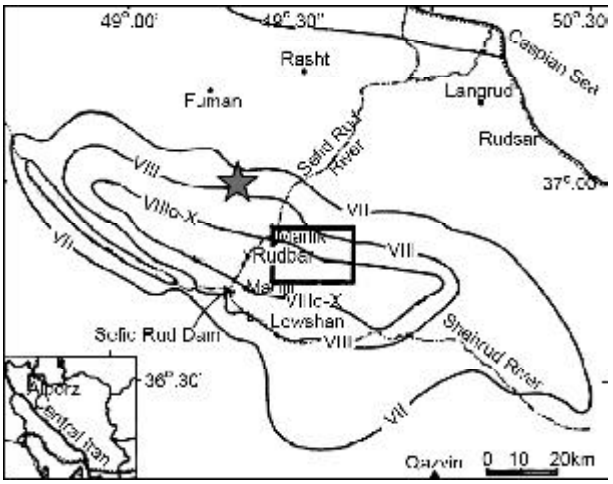

Figure 7. The intensity map of Manjil earthquake [1]. The star shows the epicenter of the earthquake and the thick quadrangle shows the study area.

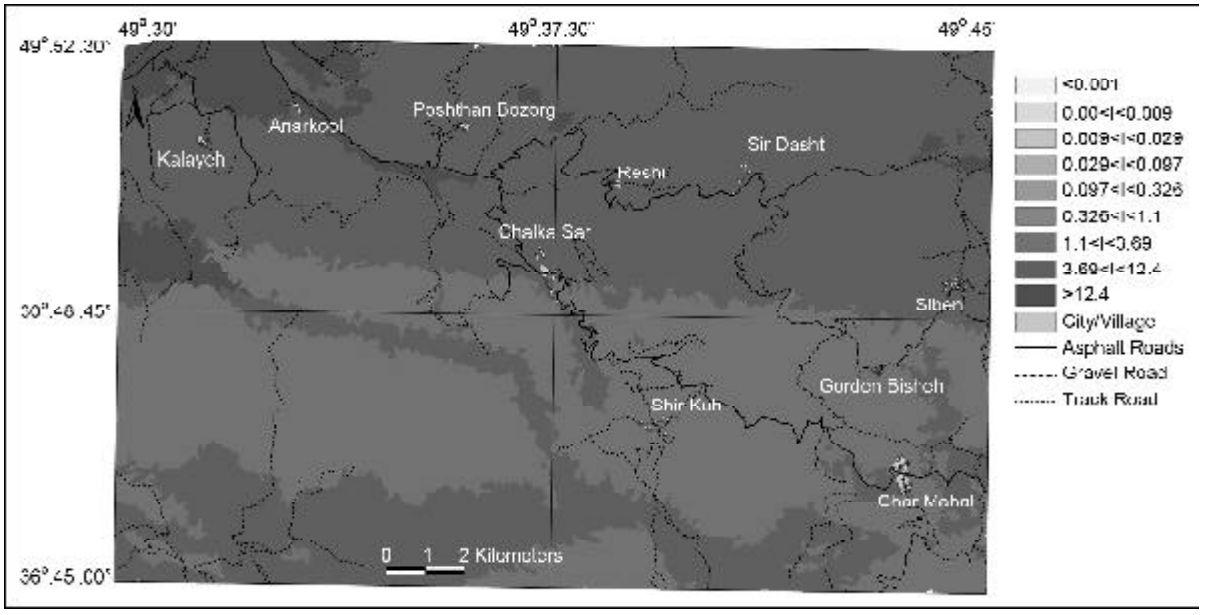

Figure 8. Arias intensity map of the study area (units are in m/s).

seen that the trend of the intensity zones are similar; but the area with higher intensity in Figure (7) is different from what is shown in Figure (8). This is resulting from the difference between the position of instrumental epicenter (star symbol in Figure (7)) and macroseismic epicenter representing the most destructed area.

In order to analyse the validity of seismic landslide hazard map, a measure, termed the 'density ratio' (*DR*) is used, which is defined as [4]:

$$DR = L/A \quad (8)$$

where L is the number/area of landslides within each hazard category expressed as a percentage of the total number/area of landslides, and A is the areal extent of the hazard category expressed as a percentage of the total study area. A good hazard map is considered to be one which provides the greatest separation into areas of high landslide density and areas of low landslide density.

To calculate the *DR* values, the Manjil earthquake triggered landslide map, see Figure (10), overlaid on seismic hazard map, see Figure (9). DR values obtained for each of the hazard categories are given in Table (5). As could be seen in Table (5), the *DR*

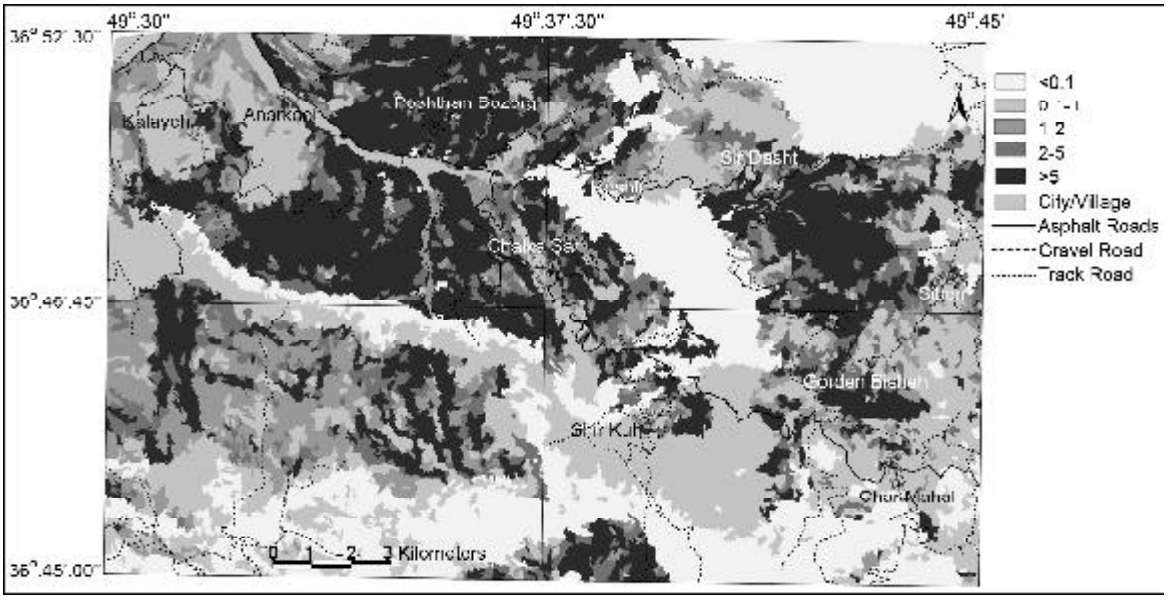

Figure 9. Seismic landslide hazard zonation map of the study area which is generated by the system (units are in cm).

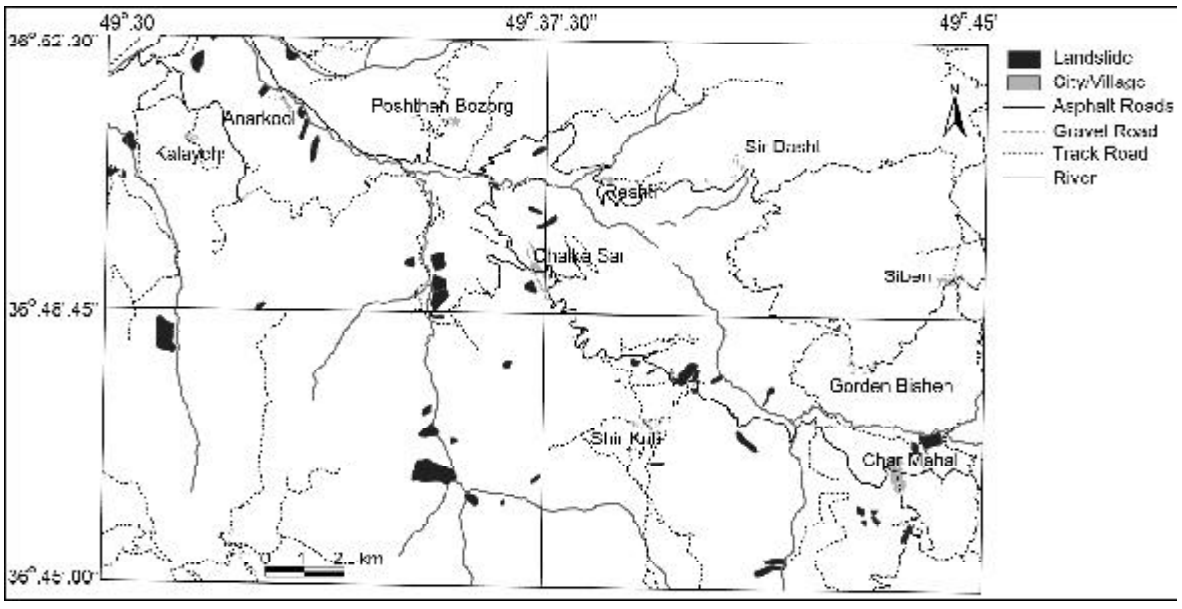

Figure 10. The map of landslides triggered by Manjil earthquake in the study area.

Table 5. DR calculations for seismic landslide hazard map of Cholkasar and Chaharmahal quadrangles.

Relative Hazard Category	Displacement (cm)	Area of Category (km2)	% Area (A)	Area of Landslides (km2)	% Landslides (L)	Density Ratio (DR)
Very High	>5	78.88	25.52	1.39	37.75	1.48
High	2-5	31.48	10.18	0.30	8.14	0.80
Moderate	1-2	37.91	12.26	0.40	10.81	0.88
Low	0.1-1	85.43	27.64	1.00	27.21	0.98
Very Low	<0.1	75.43	24.40	0.59	16.10	0.66
Sum	---	309.13	100.00	3.69	100.00	---

values increase for higher hazard levels, but the *DR* value decreases for displacement of 2 to 5cm. This could be resulted from occurrence of some landslides in low hazard category of the seismic landslide hazard map.

7. Discussion and Conclusions

Recent advances in computer hardware and software technologies have paved the road for application of rigorous analysis in regional hazard assessment using *GIS* [19]. In this study a system is developed, which models real time Arias intensity and seismic landslide hazard maps. The parameter used to generate seismic landslide hazard map is Newmark's displacement. In this study similar to previous works, there are many simplification assumption for regional assessment of Newmark's displacement, but it should be noted that this parameter do not necessarily correspond directly to measurable slope movements in the field; rather modeled displacement provide an index to correlate with field performance [14].

Shear strength typically has large spatial variability in nature even within geologic units, and assigning representative shear strength to entire units is fraught with uncertainty. In this study, Geological Strength Index (*GSI*) [8] is mainly used to estimate rock mass strength parameters. This method is grossly approximate and needs to perform a dense field work, but it could be considered as a more appropriate and rapid method in comparison with other methods (such as using triaxial tests).

The modeling procedure for Newmark's displacement calculation, however, is heavily slope driven. The effects of slope angle on the model output far outweigh the effects of modest differences in material strength; therefore, highly accurate characterizations of strength are not deemed essential [14]. For sample area, the digital map of scale 1:25000 by resolution of 10 meter is used to generate *DEM*; the map of this scale can easily show all large slopes in the area and can be used to calculate their Newmark's displacements. This data for Alborz and Central Iran (~200000km^2) is being prepared by *NCC*. Until completing data, the system uses a prepared *DEM* by a lower resolution (90 meter). Many small slopes in this *DEM* will undoubtedly merge in the greater neighboring slopes.

For testing the system, part of Manjil earthquake prone area is used. There are general mismatches between observed intensity map, see Figure (7), and the one modeled by the system, see Figure (8). There might be many sources for such uncertainties, among which the difference between instrumental and macroseismic epicenters could result in different distribution patterns. The epicenter reported for Manjil earthquake is located in the north of the earthquake fault by 20*km*; which resulted in dislocation of high hazard areas to the north of real location of the most destructed area

Another map which is generated by the system is seismic landslide hazard zonation map, see Figure (9). Comparing with triggered landslide inventory map, see Figure (10), landslides triggered by the earthquake occur mostly in high hazard zones. There are also some landslides in the low hazard zones, see Table (5). As noted in section 6, only large landslides are documented in the reconnaissance reports of the earthquake [as 5, 15]. The types of mapped major landslides are mainly slump, avalanches and flows. Most shallow, disrupted failures in brittle materials, such as rock falls and rockslides are not located, while the proposed model in this paper is most appropriately applied to thinner landslides in more brittle materials rather than to deeper landslides in softer materials.

In spite of mentioned limitations, the system provides a rapid portrayal of the extent of potentially damaging shaking and landslides following an earthquake and can be used for emergency response, loss estimation, and for public information through the media. Generation of the maps is fully automatic, triggered by any significant earthquake in Alborz and Central Iran.

Acknowledgements

The authors would like to thank R. Kardan for helping in programming in *GIS*. The authors would also like to express appreciation to M. Rakhshandeh, and V. Tajik, for helping in *GIS* works and field visits.

References

1. Berberian, M., Qorashi, M., Jackson, J.A., Priestley, K., and Wallace, T. (1992). "The Rudbar-Tarom Earthquake of June 20, 1990 in NW Iran: Preliminary Field and Seismotectonic Observations, and Its Tectonic Significance", Bulletin of the Seismological Society of America, **82**(4), 1726-1755.

2. Bray, J.D. and Travasarou, T. (2007). "Simplified Procedure for Estimating Earthquake-Induced Deviatoric Slope Displacements", *Journal of Geotechnical and Geoenvironmental Engineering*, **133**(4), 381-392.

3. Brown, E.T. (1981). "Rock Characterization, Testing and Monitoring", ISRM Suggested Methods, Pergamon, Oxford, 171-183.

4. Gee, M.D. (1992). "Classification of Landslide Hazard Zonation Methods and a Test of Predictive Capability", *6th International Symposium on Landslides*, Christchurch, New Zealand, **2**, 947-952.

5. Haeri, S.M. and Satari, M.H. (1993). "Great Landslides Triggered by Manjil Earthquake, 20 June 1990", Natural Disaster Reduction Center of Iran (In Persian).

6. Hoek, E. (1994). "Strength of Rock and Rock Masses", *ISRM News Journal*, **2**(2), 4-16.

7. Hoek, E. and Brown, E.T. (1998). "Practical Estimates of Rock Mass Strength", *Int. J. Rock Mech. Min. Sci.*, **34**, 1165-1186.

8. Hoek, E., Carranza-Torres, C., and Corkum, B. (2002). "Hoek-Brown Failure Criterion - 2002 Edition", *5th North American Rock Mechanics Symposium and 17th Tunneling Association of Canada Conference*, NARMS-TAC, 267-271.

9. Hoek, E., Kaiser P.K., and Bawden W.F. (1995). "Support of Underground Excavations in Hard Rock", Rotterdam, Balkema.

10. Hoek, E., Marinos, P., and Bennisi, M. (1998). "Applicability of the Geological Strength Index (GSI), Classification for Very Weak and Sheared Rock Masses, The Case of the Athens Schist Formation", Bulletin Eng. Geol. Env., **57**(2), 151-160.

11. Ingles, J., Darrozes, J., and Soula, J-C. (2006). "Effects of the Vertical Component of Ground Shaking on Earthquake-Induced Landslide Displacement Using Generalized Newmark Analysis", *Engineering Geology*, **86**, 134-147.

12. Jibson, R.W. (1993). "Predicting Earthquake-Induced Landslide Displacement Using Newmark's Sliding Block Analysis", Transportation Research Record 1411, Transportation Research Board, National Research Council, Washington, D.C.

13. Jibson, R.W. (2007). "Regression Models for Estimating Coseismic Landslide Displacement", *Engineering Geology*, **91**, 209-218.

14. Jibson, R.W., Harp, E.L., and Michael, J.A. (1998). "A Method for Producing Digital Probabilistic Seismic Landslide Hazard Maps: An Example from the Los Angeles", California area, U.S. Geological Survey, Open-File Report 98-113, 17p.

15. Komak Panah, A. and Hafezi Moghadas, N. (1993). "Landslide Hazard Zonation Study in Affected Area by Manjil Earthquake, 1990", *In: TC4 (1993)-Manual for Zonation on Seismic Geotechnical Hazards*, International Society for Soil Mechanics and Geotechnical Engineering.

16. Landslide Investigation Group (LIG) (2008). "Landslides Database of Iran", Forest, Range, and Watershed Management Organization, Jihad-e-Keshavarzi Ministry of Iran.

17. Mahdavifar, M. (2006). "Analytical Evaluation and Design of the System (GIS) for Seismic Landslides Hazard/Risk Management in Iran", PhD Thesis, International Institute of Earthquake Engineering and Seismology, (in Persian) 213p.

18. Mahdavifar, M. Jafari, M.K., and Zolfaghari, M.R. (2007). "The Attenuation of Arias Intensity in Alborz and Central Iran", *The 5th Int. Conf. Seis., and Earth. Eng.*, Tehran, Iran.

19. Miles, S.B. and Ho, C.L. (1999). "Rigorous

Landslide Hazard Zonation Using Newmark's Method and Stochastic Ground Motion Simulation", *Soil Dynamics and Earthquake Engineering*, **18**(4), 305-323.

20. Saygili, G. and Rathje, E.M. (2008). "Empirical Predictive Models for Earthquake-Induced Sliding Displacements of Slopes", *Journal of Geotechnical and Geoenvironmental Engineering*, **134**(6), 790-803.

21. Sharma, S. (1996). "Slope Stability Concepts", In: Abramson, L.W., Lee, T.S., Sharma, S., Royce, G.M. (Eds.), Slope, Stability and Stabilization Methods, New York, Wiley, Chapter 6.

22. Sinaiean, F. (2006). "A Study on the Strong Ground Motions in Iran (From Catalog to Attenuation Relationship)", Ph.D. Thesis, International Institute of Earthquake Engineering and Seismology, 318p.

23. USGS Homepage, Earthquake Hazard Program, Earthquake Center; http://neic.usgs.gov/neis/epic/epic.html.

24. Wald, D.J., Quitoriano, V., Heaton, T.H., Kanamori, H., Scrivner, C.W., and Worden, B. (1999). "TriNet 'ShakeMaps': Rapid Generation of Peak Ground Motion and Intensity Maps for Earthquakes in Southern California", *Earthquake Spectra*, **15**(4), 537-55.

25. Wilson, R.C. and Keefer, D.K. (1983). "Dynamic Analysis of a Slope Failure from the 1979 Coyote Lake, California Earthquake", Seismological Society of America Bulletin, **73**(3), 863-877.

26. Yassaghi, A., Salari-Rad, H., and Kanani-Moghadam, H. (2005). "Geomechanical Evaluation of Karaj Tuffs for Rock Tunneling in Tehran-Shomal Freeway, Iran", *Engineering Geology*, **77**, 83-98.

27. Zare, M., Ghafory-Ashtiany, M., and Bard, P.Y. (1999). "Attenuation Law for the Strong Motions in Iran", *Proceedings of the Third International Conference on Seismology and Earthquake Engineering*, 345-354.